Chemical Science

ROYAL SOCIETY OF CHEMISTRY

EDGE ARTICLE

View Article Online
View Journal | View Issue

Cite this: *Chem. Sci.*, 2022, **13**, 14305

All publication charges for this article have been paid for by the Royal Society of Chemistry

Received 8th September 2022
Accepted 10th November 2022

DOI: 10.1039/d2sc05008k

rsc.li/chemical-science

Spin state dependent peroxidase activity of heme bound amyloid β peptides relevant to Alzheimer's disease†

Arnab Kumar Nath, Madhuparna Roy, Chinmay Dey, Abhishek Dey* and Somdatta Ghosh Dey *

The colocalization of heme rich deposits in the senile plaque of Aβ in the cerebral cortex of the Alzheimer's disease (AD) brain along with altered heme homeostasis and heme deficiency symptoms in AD patients has invoked the association of heme in AD pathology. Heme bound Aβ complexes, depending on the concentration of the complex or peptide to heme ratio, exhibit an equilibrium between a high-spin mono-His bound peroxidase-type active site and a low-spin bis-His bound cytochrome b type active site. The high-spin heme–Aβ complex shows higher peroxidase activity than free heme, where compound I is the reactive oxidant. It is also capable of oxidizing neurotransmitters like serotonin in the presence of peroxide, owing to the formation of compound I. The low-spin bis-His heme–Aβ complex on the other hand shows enhanced peroxidase activity relative to high-spin heme–Aβ. It reacts with H_2O_2 to produce two stable intermediates, compound 0 and compound I, which are characterized by absorption, EPR and resonance Raman spectroscopy. The stability of compound I of low-spin heme–Aβ is accountable for its enhanced peroxidase activity and oxidation of the neurotransmitter serotonin. The effect of the second sphere Tyr10 residue of Aβ on the formation and stability of the intermediates of low-spin heme–Aβ has also been investigated. The higher stability of compound I for low-spin heme–Aβ is likely due to H-bonding interactions involving Tyr10 in the distal pocket.

1. Introduction

Alzheimer's disease (AD) is a neurodegenerative disorder, which is clinically characterized by progressive loss of brain functions.[1–4] It is the most common form of senile dementia with symptoms like confusion, rapid mood swings, apraxia and long-term memory loss that eventually culminates in death.[4–6] Although the exact cause of AD has remained elusive to date, research over the years into the etiopathology of this disease has resulted in the proposal of some important hypotheses, among which the "amyloid cascade hypothesis" is most widely known.[4,7,8] According to this hypothesis, the main histopathological criterion of AD is the extracellular deposition of amyloid fibrils made up of the amyloid β (Aβ) peptide to form structures known as senile plaques,[3,4,7–9] which are neurotoxic. This small peptide is generated from a transmembrane protein called the amyloid precursor protein (APP) by the action of secretase enzymes.[4,6,10] The Aβ peptides containing 40 and 42 amino acids *i.e.*, Aβ(1-40) and Aβ(1-42) respectively, are the most abundant in the AD brain.[4,10] Apart from Aβ, transition metals like Cu and Zn are also found within the senile plaques, both of which have been reported to strongly bind the Aβ peptide.[4,9–12] Cu, as a redox active metal, has been proposed to cause oxidative stress that can lead to neuronal cell damage, nucleic acid adduct formation, neurotransmitter oxidation, *etc.*[13–18] Zn, on the other hand, has significant contribution to Aβ deposition.[4,10] Thus, over the last few decades, a number of small molecular inhibitors of Aβ aggregation/production and Cu and Zn chelators have been used in therapeutic trials but unfortunately none have been able to provide any symptomatic relief.[19–22] However, it should be noted that more recent investigations into potential anti-AD drugs targeting metal homeostasis have led to the design and application of highly specific metal chelators, particularly for Cu(II), such as TDMQ20, which has shown encouraging outcomes like improvements in cognition in transgenic and nontransgenic murine models of AD.[23,24]

Although the importance of Aβ in the AD paradigm is undeniable, in light of the drawbacks of the abovementioned hypotheses in adequately explaining the cause and progression of the disease, the focus has been shifted towards determining an alternative origin of AD. One such recent hypothesis regarding AD pathogenesis is centered on the heme moiety that is found all over the human body including the brain.[25–27] The perturbation of heme (and hence iron) metabolism is observed in the AD brain, which manifests itself as heme deficiency

School of Chemical Sciences, Indian Association for the Cultivation of Science, 2A & 2B, Raja S. C. Mullick Road, Jadavpur, Kolkata 700032, India. E-mail: icsgd@iacs.res.in

† Electronic supplementary information (ESI) available. See DOI: https://doi.org/10.1039/d2sc05008k

symptoms such as lower levels of heme *a* (26%), a possible compensatory increase in heme *b* (250%), mitochondrial complex IV dysfunction, unregulated iron accumulation, over expression of heme oxygenase, biliverdin reductase A, ferrochelatase, elevated levels of heme degradation products like bilirubin *etc.*[4,22,27–31] Apart from the brain, changes in the iron and heme homeostasis are also observed in the blood of AD patients in the form of lowering of haemoglobin and peripheral iron levels as well as identification of anaemia, which is common in elderly individuals, as a risk factor for the disease.[32–34] All these findings are suggestive of a link between the heme regulatory pathway and AD. Further support for such a causal relationship between heme and AD comes from reports of spatial overlap between heme rich deposits and Aβ containing senile plaques in the AD brain and presence of both these structures in the vicinity of microvessels.[35,36] In fact, experiments on a murine AD model show vascular Aβ deposition, *i.e.*, cerebral amyloid angiopathy (CAA) can damage microvessels (microhemorrhages) and have haemolytic effects, which may be a source of free heme accumulation in the AD brain.[37] Heme in the form of hemoglobin has also been found to co-localize with the senile plaques with its levels being higher in AD associated brain regions like the hippocampus, parietal grey matter, parietal white matter and inferior temporal gyri.[31,38] Hence, multiple lines of evidence provide credibility to the heme based hypothesis and have even led to much research effort being directed towards studying how heme and the plaque forming Aβ peptide interact with each other and the consequences thereof. The binding of heme to Aβ has been proposed to result in the depletion of regulatory heme, which may explain the observation of heme deficiency symptoms in AD.[4,27,31,39] Recent Raman imaging of AD brain tissue has revealed that, heme present in Aβ plaques in the brain tissue resembles a six coordinated low-spin species that may possibly be a bis-His low-spin heme–Aβ species.[40]

Heme has been shown to bind to the Aβ peptide through the histidine side chain and depending on the cofactor to peptide ratio or concentration, heme–Aβ complexes can have different coordination environments and spin states.[22,41,42] When heme and Aβ are present in 1 : 1 stoichiometry and at low concentrations, the resultant complex is a high-spin one with an axial His ligation and a weakly bound *trans*-axial water derived ligand (Fig. 1). In the presence of H_2O_2, this high-spin heme–Aβ complex shows greater peroxidase activity than free heme. It goes through an Fe^{IV}=O porphyrin π cation radical species called compound I in the catalytic cycle, which has been found to be responsible for the oxidation of the neurotransmitter serotonin, an essential neurotransmitter that takes part in important functions like the formation of new memory, cognitive functions, mood stabilization and so on.[43] The formation and stability of this high valent transient intermediate are influenced by the distal Arg5 residue by virtue of its pull effect, while the non-coordinating Tyr10 residue hastens the decay process *i.e.*, it is redox active. When Aβ is present in excess or the concentration of heme–Aβ is high, the active site transforms to a cyt. b like a low-spin site with bis His coordination[22,42] (Fig. 1). Moreover, we have previously characterized the active site of heme–Aβ in small aggregates or oligomers by resonance Raman spectroscopy that shows a significant amount of low-spin component for the heme–Aβ complex.[44] This low-spin complex has been found to exhibit even greater peroxidase activity than the high-spin analogue.

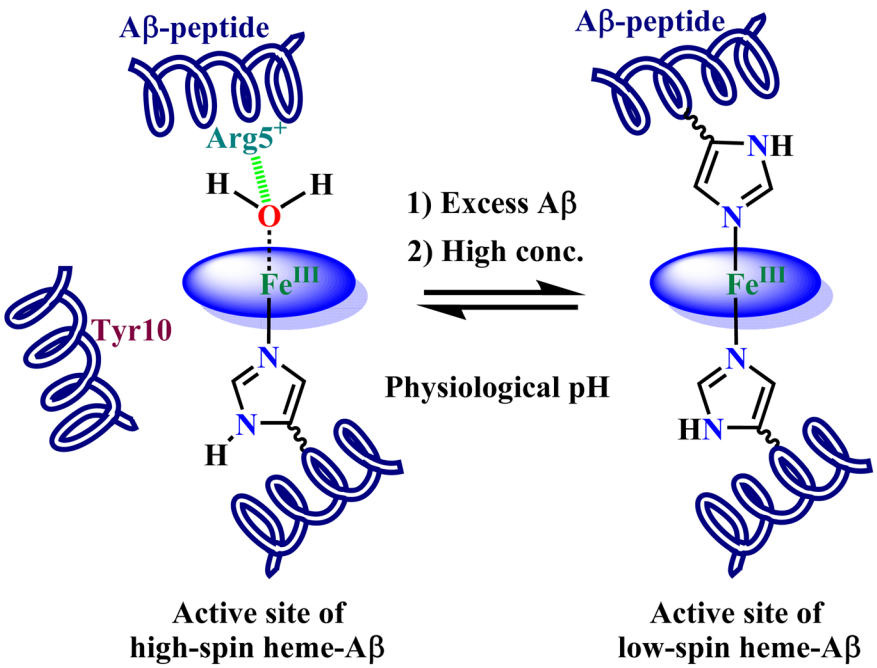

Fig. 1 Condition dependent equilibrium between high-spin mono-His heme–Aβ (LHS) and low-spin bis-His heme–Aβ (RHS) at physiological pH.

In the present study, we observe that this enhanced peroxidase activity is associated with the reaction intermediate compound I. In fact, the reaction of low spin heme–Aβ and H_2O_2 produces two intermediates compound 0, which is an Fe^{III}–OOH species, and compound I respectively, which have been trapped and characterized using absorption, EPR and resonance Raman spectroscopy. The role of the second sphere Tyr10 residue has also been probed extensively showing how it differs from the analogous high-spin heme–Aβ. The fate of compound I in the presence of the neurotransmitter serotonin has been investigated as well. It has been found that a stable compound I of low-spin heme–Aβ resulting in its higher peroxidase activity is the active oxidant for the neurotransmitter serotonin oxidation, a key pathological feature of AD.[45–51] Since, it is well established that Aβ oligomers are more neurotoxic than larger aggregates[52–57] and given the fact that these oligomers contain a significant amount of low-spin heme–Aβ, higher peroxidase activity of low-spin heme–Aβ resulting in the oxidation of neurotransmitters can potentially lead to neurodegeneration associated with AD.

2. Results and analysis

2.1. Peroxidase activity of low-spin heme–Aβ and the Tyr10Phe mutant

The peroxidase activity of the wild type (WT) low-spin heme–Aβ and its site directed tyrosine mutant (Tyr10Phe) is monitored by absorption spectroscopy, using 3,5,3′,5′-tetramethyl benzidine (TMB) as the substrate by following the 652 nm band (Fig. S1†). Starting from a colorless solution, the appearance of a blue-colored solution with absorption peaks at 370 nm and 652 nm indicates the formation of a charge-transfer complex (Scheme S1†), which then converts to a yellow solution, indicative of the formation of a diamine complex. This indicates a two electron oxidation of TMB (Fig. S2A and S3A, Scheme S1†).[58,59] The six-coordinated bis-His low-spin heme–Aβ complex exhibits approximately ~3 times enhanced peroxidase activity relative to the five-coordinated mono-his high-spin heme–Aβ complex (Fig. 2A), consistent with previous reports.[60–62] Interestingly, in the absence of the tyrosine residue at the 10th position (Tyr10), low-spin heme–Aβ exhibits about four times enhanced peroxidase activity relative to the native heme–Aβ complex (Fig. 2B).

In naturally occurring peroxidases, the main active oxidant responsible for peroxidase activity is the high valent ferryl porphyrin π-cation radical (Fe^{IV}=OPor$^{\bullet+}$), named compound I.[60,63–65] The low-spin heme–Aβ shows significant enhancement in the rate of TMB oxidation (peroxidase activity, formation of the 652 nm band) in the presence of H_2O_2 relative to control experiments, *i.e.* TMB + H_2O_2, TMB + H_2O_2 + heme, and TMB + H_2O_2 + Aβ (Fig. S4†), negating the involvement of an uncontrolled radical process generated by H_2O_2 or adventitious metal traces in the oxidation process. Our group has recently trapped and characterized the compound I species in the peroxidase cycle of high-spin heme–Aβ, akin to native peroxidases.[19]

2.2. Reaction of low-spin heme–Aβ and H_2O_2

2.2.1. Absorption spectroscopy

Low-spin heme–Aβ (WT) + H_2O_2. The low-spin heme–Aβ(WT) complex shows a characteristic Soret band at 414 nm and Q-bands at 535 nm and 566 nm (Fig. 3A, S5 and S6†). The reaction of low-spin heme–Aβ with H_2O_2 causes a decrease in the intensity of these absorption bands along with simultaneous formation of new bands at 600 nm and 670 nm (Fig. S5† and 3A–C). The kinetic traces at 600 and 670 nm indicate that the 600 nm band has a faster rate of formation compared to the 670 nm band (Fig. 3D). The formation of the bands at 600 and 670 nm follows 1st order kinetics with a rate of formation of 1.6 × 10^{-2} s^{-1} and 8.5 × 10^{-3} s^{-1}, respectively. Unlike the band at 670 nm, the 600 nm band decays during the course of the reaction (Fig. 3D). These observations likely indicate that the reaction of heme–Aβ and H_2O_2 produces two reaction intermediates with characteristic bands at 600 nm and 670 nm. According to existing literature reports, the absorption band at around 650–675 nm is typically characteristic of a ferryl porphyrin π-cation radical (Fe^{IV}=OPor$^{\bullet+}$) or compound I.[66–70] Note that compound I of heme–Aβ high-spin species exhibits a characteristic band at ~675 nm.[19] The absorption band at

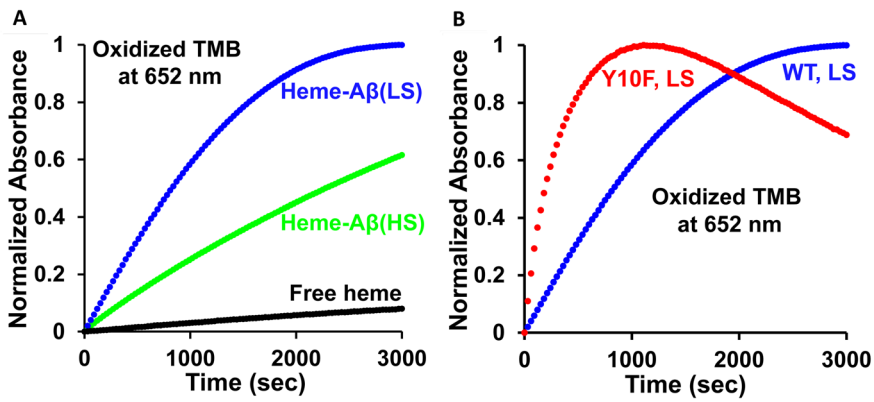

Fig. 2 Comparison of the rate of peroxidase activity (TMB oxidation) of (A) wild type low-spin heme–Aβ (WT, LS) (blue), wild type high-spin heme–Aβ (WT, HS) (green) and free heme (black); (B) wild type low-spin heme–Aβ (WT, LS) (blue) and low-spin heme–Aβ Tyr10 mutant (Y10F, LS) (red); monitored at 652 nm in 100 mM phosphate buffer at pH 7.6.

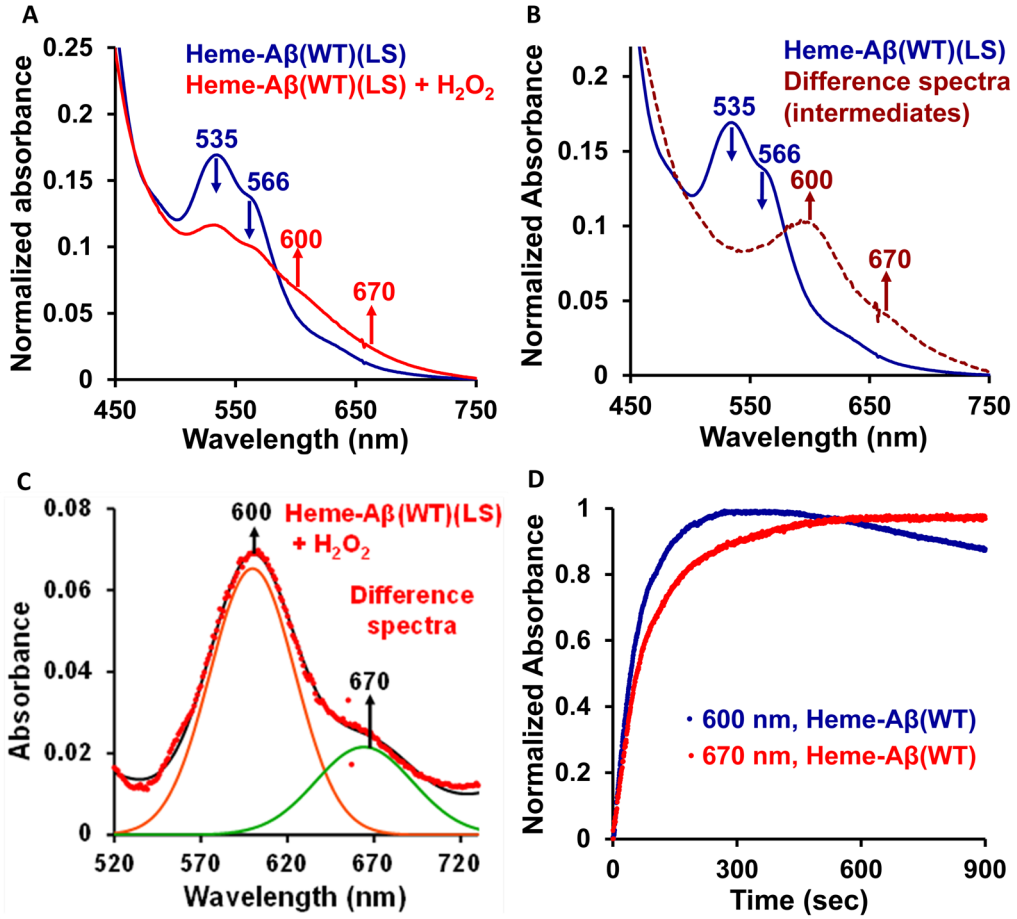

Fig. 3 (A) Absorption spectrum of low spin heme–Aβ(WT) (blue), for the reaction of low-spin heme–Aβ(WT) with H_2O_2 (red); (B) absorption spectrum of low-spin heme–Aβ(WT) (blue) and difference spectrum obtained by subtracting the spectrum of low-spin heme–Aβ(WT) from the spectrum of the reaction mixture of low-spin heme–Aβ(WT) + H_2O_2 (brown, dashed line) indicates the appearance of distinct bands for the intermediates at 600 nm and 670 nm; (C) difference absorption spectrum (Q-band) of low-spin heme–Aβ(WT) with H_2O_2 (red dotted line) and simulated spectrum (black solid line). The simulated line shows the appearance of two bands upon reaction of low-spin heme–Aβ(WT) with H_2O_2, one at 600 nm and the other at 670 nm. (D) Overlay of reaction kinetics for the 600 nm (blue) and 670 nm (red) bands formed in the reaction of low spin heme–Aβ(WT) with H_2O_2. The reaction is done in 100 mM phosphate buffer at pH 7.6.

670 nm for low-spin heme bound Aβ upon reaction with H_2O_2 may therefore likely correspond to a stable compound I species, while the band at 600 nm, which forms prior to compound I, may be attributed to an Fe^{III}–OOH or compound 0 species.

Low-spin heme–Aβ(Tyr10Phe) + H_2O_2. The Tyr10Phe mutant (Y10F) shows a characteristic Soret band at 414 nm and Q-bands at 535 and 566 nm (Fig. 4A, S7 and S8†). Upon reaction with H_2O_2, the low-spin heme–Aβ Tyr10Phe mutant (Y10F) shows a decrease in the intensity of these characteristic absorption bands with concomitant formation of new bands at 600 nm and 670 nm (Fig. S7† and 4A–C), similar to the native low-spin heme–Aβ complex. The formation of the 600 nm band occurs prior to the 670 nm band (Fig. 4D), analogous to the native complex. Thus, the bands at 600 and 670 nm for Tyr10Phe (Y10F) may correspond to compound 0 and compound I respectively, similar to the native complex. However, a notable feature of the Tyr10Phe (Y10F) mutant of low-spin heme–Aβ is a faster rate of formation as well as a faster decay of the band at 600 nm, attributed to compound 0, in contrast to the native heme–Aβ complex (Fig. S9†). This indicates a possible second sphere effect exerted by Tyr10 in the formation of the reaction intermediates and hence on the peroxidase activity exhibited by low-spin heme–Aβ.

2.2.2. EPR spectroscopy. The EPR spectra of the frozen samples of low-spin heme–Aβ Tyr10Phe (Y10F) in the presence of H_2O_2 are recorded at 77 K at different times during the course of the reaction (Fig. 5). The low-spin Tyr10Phe mutant (Y10F) shows a weak EPR signal at 77 K. The reaction of Tyr10Phe (Y10F) and H_2O_2 produces a rhombic EPR signal after ~3 min with g values observed at ~2.42 (g_1) and 2.06 (g_2), corresponding to a low-spin Fe^{III} species (Fig. 5, red spectrum). Such a rhombic low-spin Fe^{III} EPR signal is characteristic of an end-on low spin Fe^{III}–OOH species or compound 0, similar to the previous reports of various heme proteins such as myoglobin, hemoglobin, cytP450 and several Fe-porphyrin model complexes.[71–74] Note that the third rhombic EPR signal corresponding to g_3 for compound 0 could not be resolved, similar to some reported systems, where the signal is too weak to be observed at 77 K.[71]

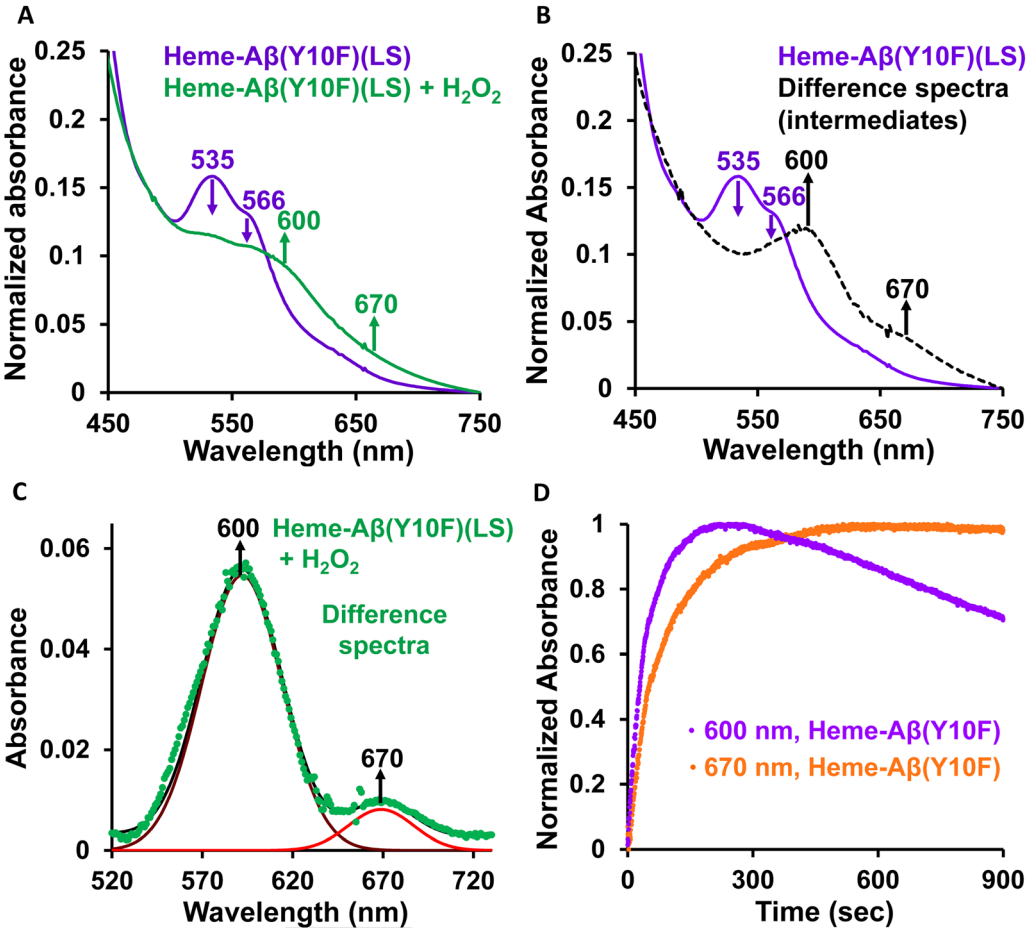

Fig. 4 (A) Absorption spectrum of the low-spin heme–Aβ Tyr10 mutant (Y10F) (purple), for the reaction of the low-spin heme–Aβ Tyr10 mutant (Y10F) with H_2O_2 (green); (B) absorption spectrum of the low-spin heme–Aβ Tyr10 mutant (Y10F) (purple) and difference spectrum obtained by subtracting the spectrum of the low-spin heme–Aβ Tyr10 mutant (Y10F) from the spectrum of the reaction mixture of the low-spin heme–Aβ Tyr10 mutant (Y10F) + H_2O_2 (black, dashed line) indicates the appearance of distinct bands for the intermediates at 600 nm and 670 nm; (C) difference absorption spectrum (Q-band) of low spin heme–Aβ(Y10F) with H_2O_2 (green dotted line) and simulated spectrum (black solid line). The simulated line shows the appearance of two bands upon reaction of low spin heme–Aβ(Y10F) with H_2O_2, one at 600 nm and the other at 670 nm. (D) Overlay of reaction kinetics for the 600 nm (purple) and 670 nm (orange) bands formed in the reaction of the low spin heme–Aβ Tyr10 mutant (Y10F) with H_2O_2. The reaction is done in 100 mM phosphate buffer at pH 7.6.

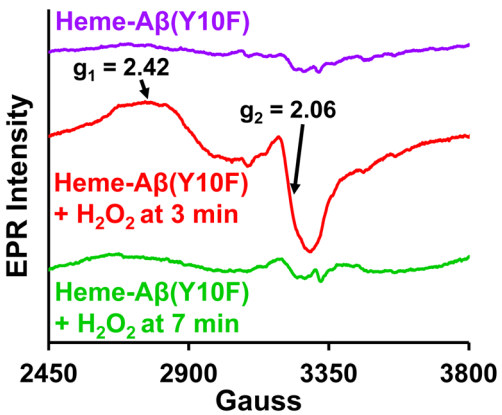

Fig. 5 EPR spectra of the low spin heme–Aβ Tyr10 mutant (Y10F) (purple), for the reaction of the low spin heme–Aβ Tyr10 mutant (Y10F) with H_2O_2 at ~3 min (red) and at ~7 min (green). The reaction is done in 100 mM phosphate buffer at pH 7.6 and EPR data are recorded at 77 K.

When the reaction proceeds further (~7 min), the low-spin Fe^{III} EPR signal characteristic of compound 0 nearly disappears, indicative of the decay of this species, consistent with absorption spectroscopy (Fig. 4D). Any characteristic feature of compound I could not be detected at 77 K (Fig. 5, red or green spectra) (usually detected below 30 K),[75,76] possibly due to spin relaxation, imposed by the interaction between the porphyrin ring radical and the heme–Fe center.[77]

2.2.3. Resonance Raman spectroscopy

Low-spin heme–Aβ (WT) + H_2O_2. The putative reaction intermediates, compound 0 and compound I, formed during the reaction between heme–Aβ (WT and Tyr10Phe) and H_2O_2, have characteristic vibrational features and are probed by resonance Raman spectroscopy. The resonance Raman spectra of frozen solution of low-spin heme–Aβ(WT) and H_2O_2 are obtained by using an excitation wavelength of 413.1 nm. The low-spin $heme^{III}$–Aβ(WT) complex shows characteristic resonance Raman marker bands ν_4 (oxidation state) and ν_2 (spin state) at

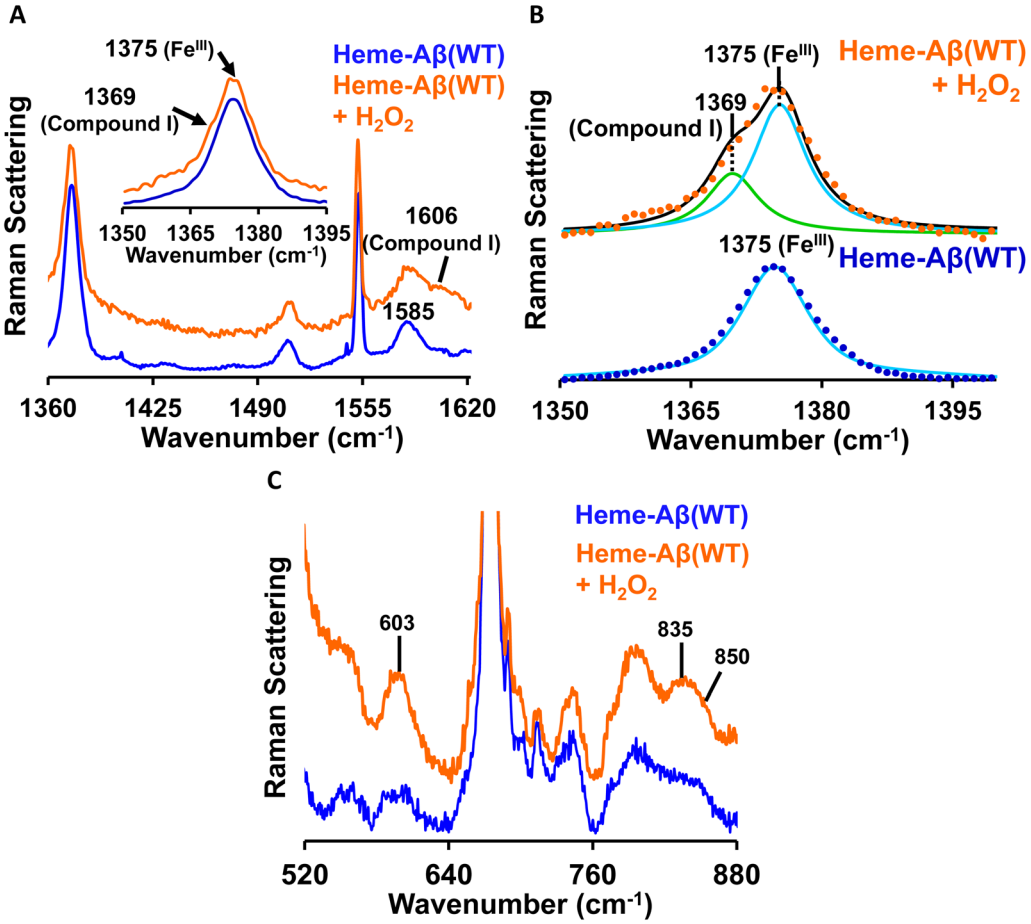

Fig. 6 (A) High frequency region of the resonance Raman spectra of low-spin heme–Aβ(WT) (blue) and for the reaction of low-spin heme–Aβ(WT) with H_2O_2 (orange); inset: the ν_4 region of the higher frequency region of the resonance Raman spectra of low spin heme–Aβ(WT) (blue) and for the reaction of low spin heme–Aβ(WT) with H_2O_2 (orange); (B) data at the bottom: experimental ν_4 region of the high frequency region of the resonance Raman spectra of low-spin heme–Aβ(WT) (blue dotted line) and simulated spectrum (cyan solid line). Simulation shows only one band at 1375 cm^{-1}. Data on the top: experimental ν_4 region of the high frequency region of the resonance Raman spectra of low-spin heme–Aβ(WT) + H_2O_2 (orange dotted line) and simulated spectrum (black solid line). Simulation shows the appearance of a new band at 1369 cm^{-1} along with 1375 cm^{-1}; (C) low frequency region of the resonance Raman spectra for the reaction of low spin heme–Aβ(WT) (blue) and low spin heme–Aβ(WT) and H_2O_2 (orange). The reaction is done in 100 mM phosphate buffer at pH 7.6 and data are obtained with an excitation wavelength of 413.1 nm (5 mW) at 77 K.

1375 and 1585 cm^{-1} respectively (Fig. 6A). In addition to the marker bands characteristic of the resting state, the addition of H_2O_2 produces broadening of the oxidation state marker band *i.e.*, the ν_4 band due to the presence of a shoulder at 1369 cm^{-1} along with the appearance of a new band in the ν_2 region at 1606 cm^{-1} (Fig. 6A, inset). The fitting of the ν_4 region shows bands at 1369 and 1375 cm^{-1} (Fig. 6B). These marker bands at 1369 cm^{-1} and 1606 cm^{-1} suggest the formation of a ferryl porphyrin π-cation radical (Fe^{IV}=OPor$^{\bullet+}$) *i.e.* compound I,[19,78–81] consistent with the absorption data (band at 670 nm, Fig. 3).

The reaction of low-spin heme–Aβ(WT) with H_2O_2 produces bands at 603 cm^{-1}, 835 cm^{-1} and 850 cm^{-1} in the lower frequency region (Fig. 6C). When the reaction is carried out in deuterated medium, the bands at 603 cm^{-1} and 835 cm^{-1} shift to 588 cm^{-1} and 816 cm^{-1} respectively (Fig. S10†). However, the band at 850 cm^{-1} remains unperturbed in deuterated medium (Fig. S10†). Bands in the ~550–610 cm^{-1} and 800–830 cm^{-1} region are characteristic of the Fe–O and O–O stretching of compound 0 (Fe^{III}–OOH), respectively,[82–84] whereas bands at ~830–850 cm^{-1} represent the Fe–O vibration of compound I for neutral (histidine/imidazole) or weakly bound axial ligand containing systems.[19,81,82,85] Note that such a high H/D isotope effect can be observed for compound 0 (Fe^{III}–OOH) like systems and can be attributed to the mixing or mode-coupling of the fundamental O–H stretching with porphyrin vibrations.[82] It is to be noted that compound I of high-spin heme–Aβ is characterized by the ν_4 band at 1368 cm^{-1} and the Fe–O stretching at 843 cm^{-1} (Table 1) that undergoes a 40 cm^{-1} downshift upon isotopic substitution of oxygen (O^{16}/O^{18}) of peroxide.[19] Bands at 603 cm^{-1} and 835 cm^{-1} therefore represent ν_{Fe-O} and ν_{O-O} vibrations for compound 0 of heme–Aβ for low-spin heme–Aβ(WT) (Fig. 6C and S10†). On the other hand, the band at 850 cm^{-1} along with new marker bands at 1369 cm^{-1} (ν_4) and 1606 cm^{-1} (ν_2) (Fig. 6 and S10†) may indicate the formation of compound I for low-spin heme–Aβ(WT).

Table 1 Comparison of the higher frequency region of resonance Raman of the intermediates formed in the reaction of heme–Aβ (HS and LS) and peroxides[a]

	ν_4 region (cm^{-1})			ν_2 region (cm^{-1})		
Heme–Aβ complexes	Fe^{III}	Cmpd 0	Cmpd I	Fe^{III}	Cmpd 0	Cmpd I
Heme–Aβ(Y10F)(HS)	1375	—	1368	1575	—	—
Heme–Aβ(WT)(LS)	1375	1375	1369	1585	—	1602
Heme–Aβ(Y10F)(LS)	1375	1375	1369	1585	1591	1602

[a] Fe^{III} = resting state, Cmpd 0 = compound 0 (Fe^{III}–OOH), and Cmpd I = compound I (Fe^{IV} = OPor$^{\bullet+}$).

Low-spin heme–Aβ(Tyr10Phe) + H_2O_2. The reaction of low-spin heme–Aβ(Tyr10Phe) with H_2O_2 is monitored by resonance Raman spectroscopy. Resonance Raman spectra obtained at different times during the course of the reaction of low-spin heme–Aβ(Tyr10Phe) and H_2O_2 are shown in Fig. 7. The addition of H_2O_2 initially shifts the ν_2 band at 1585 cm^{-1} for low-spin $heme^{III}$–Aβ to 1591 cm^{-1} with no observed change in the ν_4 band at 1375 cm^{-1} (Fig. 7), which indicates the formation of a new low-spin Fe^{III} species consistent with EPR spectroscopy. Moreover, in the later phase of the reaction a new set of

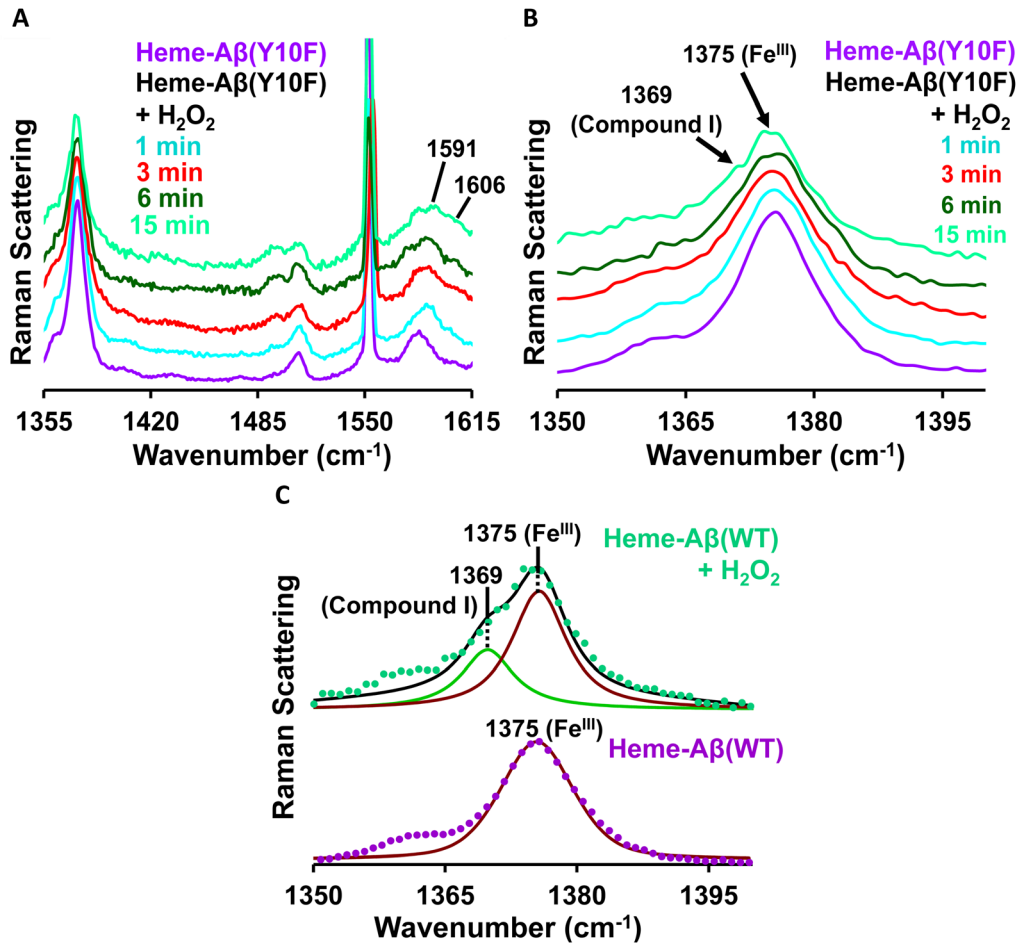

Fig. 7 (A) High frequency region of the resonance Raman spectra of the low spin heme–Aβ Tyr10 mutant (Y10F) (purple), low spin heme–Aβ Tyr10 mutant (Y10F) and H_2O_2 at 1 min (cyan), 3 min (red), 6 min (dark green) and 15 min (light green); (B) the ν_4 region of the higher frequency region of the resonance Raman spectra of the low spin heme–Aβ Tyr10 mutant (Y10F) (purple), for the reaction of the low spin heme–Aβ Tyr10 mutant (Y10F) and H_2O_2 at 1 min (cyan), 3 min (red), 6 min (dark green) and 15 min (light green); (C) data at the bottom: experimental ν_4 region of the high frequency region of the resonance Raman spectra of low-spin heme–Aβ(Y10F) (purple dotted line) and simulated spectrum (brown solid line). Simulation shows only one band at 1375 cm^{-1}. Data on the top: experimental ν_4 region of the high frequency region of the resonance Raman spectra of low-spin heme–Aβ(Y10F) + H_2O_2 (light green dotted line) and simulated spectrum (black solid line). Simulation shows the appearance of a new band at 1369 cm^{-1} along with 1375 cm^{-1}. The reaction is done in 100 mM phosphate buffer at pH 7.6 and data are obtained with an excitation wavelength of 413.1 nm (5 mW) at 77 K.

bands at 1369 cm^{-1} in the ν_4 region and 1606 cm^{-1} in the ν_2 region appear (Fig. 7, Table 1), similar to native low-spin heme–Aβ(WT), which is characteristic of compound I formation.

In the lower frequency region, the aforementioned reaction produces bands at 603 cm^{-1} and 835 cm^{-1} in the initial phase. However, with time, these bands lose their intensity and the band at 850 cm^{-1} becomes more prominent (Fig. 8A). When the reaction of low-spin heme–Aβ(Tyr10Phe) and H_2O_2 is performed in deuterated medium, a shift of the bands from 603 cm^{-1} to 588 cm^{-1} and 835 cm^{-1} to 816 cm^{-1} is observed (Fig. 8B and S11†), similar to wild type low-spin heme–Aβ (Fig. S10†). In addition, when the same reaction is performed in isotope labelled solvent (H_2O^{18}), it only produces a shift of the band at 850 cm^{-1} to 809 cm^{-1} with no perturbation of the bands at 603 cm^{-1} and 835 cm^{-1} (Fig. 8C and S12†). Note that to minimize the interference of the background noise from quartz, charcoal data are subtracted from the experimental data of low-spin heme–Aβ Tyr10 mutant (Y10F) + H_2O_2. Thus the bands at 603 cm^{-1} and 835 cm^{-1} that undergo a large H/D downshift but remain unperturbed in isotope labelled solvent (H_2O^{18}) therefore represent the ν_{Fe-O} and ν_{O-O} vibrations of compound 0 respectively.[82] However, the band at 850 cm^{-1} that undergoes a 41 cm^{-1} downshift in isotope labelled solvent (H_2O^{18}) corresponds to ν_{Fe-O} of compound I.[19,81,82,85,86] Thus, the reaction intermediates, compound 0 and compound I originating from low-spin heme–Aβ(Tyr10Phe) are confirmed by isotopic substitution of proton (H/D) and oxygen ($O^{16/18}$) of H_2O_2 (Fig. 9).

2.2.4. Kinetics. The reaction kinetics of compound 0 and compound I depends on the concentration of protons in the medium.[64,65] The formation of compound 0 (Fe^{III}–OOH) requires the detachment of a proton from the Fe^{III}–H_2O_2 precursor[64,65] and the formation of compound I from Fe^{III}–OOH requires proton assisted O–O bond heterolysis.[64,65,87]

The rate of compound 0 formation (600 nm band) for low-spin heme–Aβ(WT) decreases in deuterated medium with respect to the reaction in aqueous medium and the observed k_H/k_D value is ~3 (Fig. 10). This is indicative of involvement of a proton in the formation of compound 0. The rate of

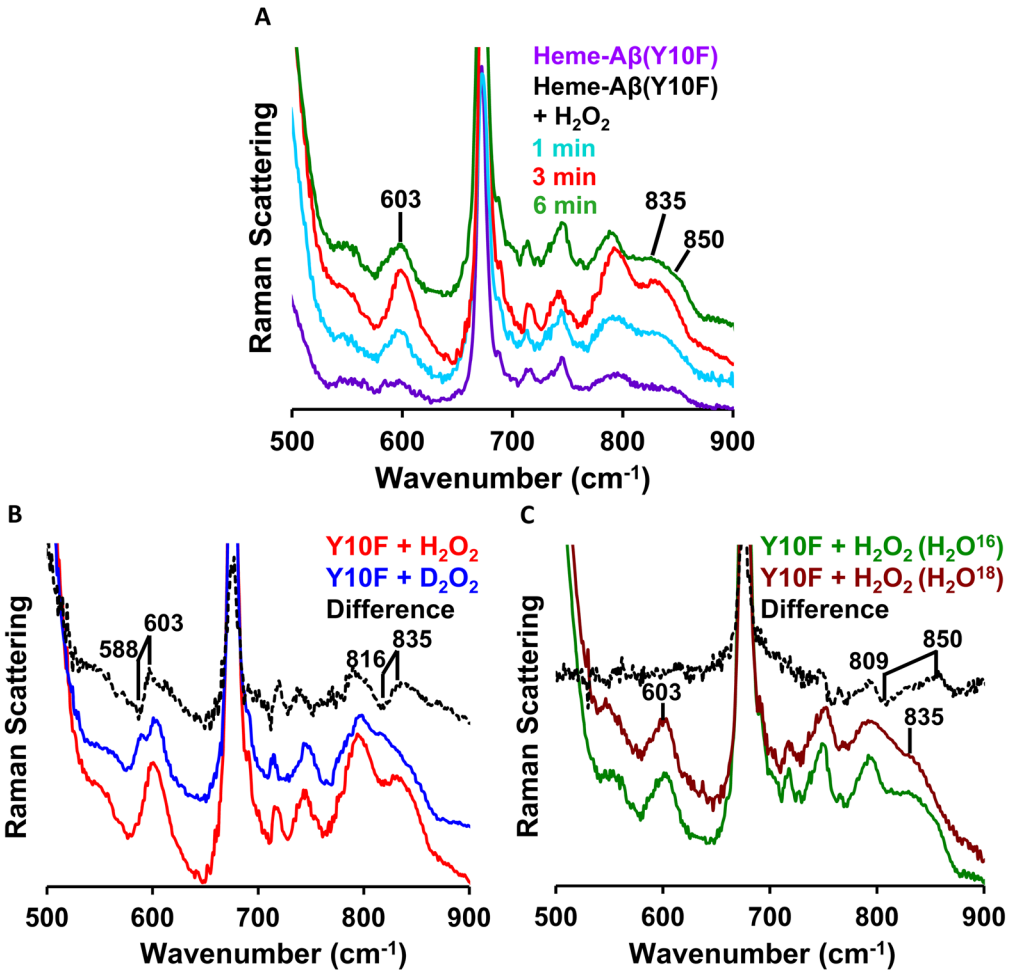

Fig. 8 Low frequency region of the resonance Raman spectra of (A) the low-spin heme–Aβ Tyr10 mutant (Y10F) (purple), low-spin heme–Aβ Tyr10 mutant (Y10F) and H_2O_2 at 1 min (cyan), 3 min (red) and 6 min (green); (B) for the reaction of the low-spin heme–Aβ Tyr10 mutant (Y10F) and H_2O_2 (red) and low-spin heme–Aβ Tyr10 mutant (Y10F) and D_2O_2 (blue); (C) for the reaction of the low-spin heme–Aβ Tyr10 mutant (Y10F) and H_2O_2 (in H_2O^{16}) (green) and low-spin heme–Aβ Tyr10 mutant (Y10F) and H_2O_2 (in H_2O^{18}) (brawn). The reaction is done in 100 mM phosphate buffer at pH 7.6 and data are obtained with an excitation wavelength of 413.1 nm (5 mW) at 77 K.

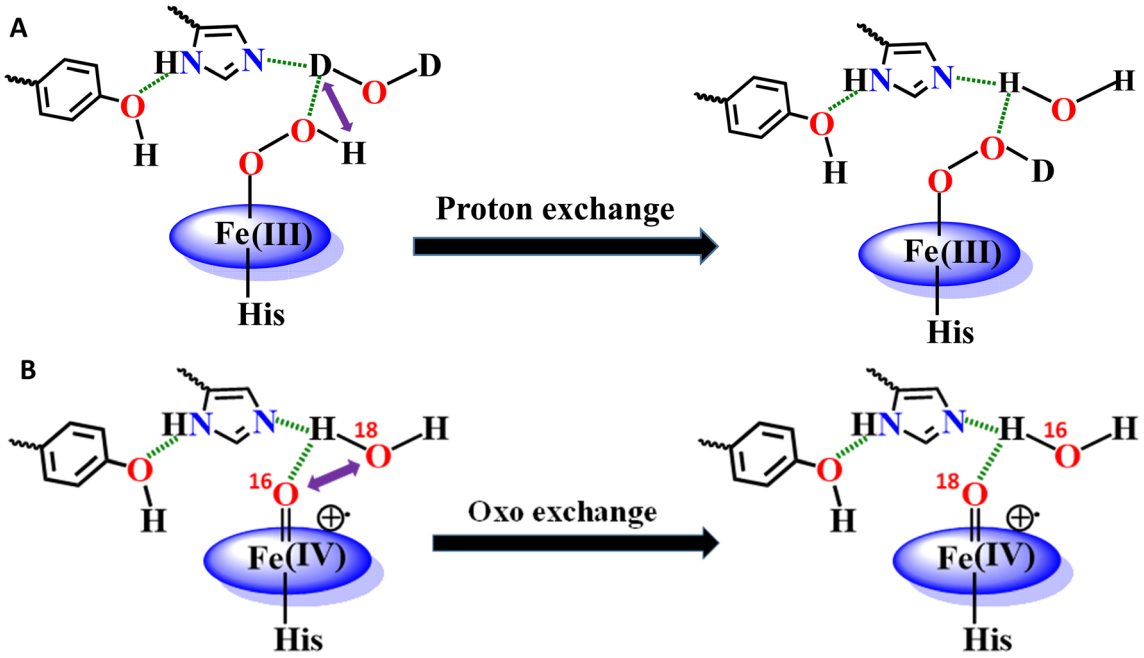

Fig. 9 Schematic diagram representing (A) proton ($^{1}H-^{2}H$) exchange of compound 0 and (B) oxo ($^{16}O-^{18}O$) exchange of compound I of heme–Aβ low spin.

compound I formation (670 nm band) for low-spin heme–Aβ exhibits a high k_H/k_D of ~3.5 (Fig. 10). The large kinetic isotope effect (KIE) for low-spin heme–Aβ may thus suggest that in the low-spin complex, there is no preorganized proton transfer residue like arginine (Arg5) to assist the O–O bond heterolysis of compound 0 to form compound I.[19,64] Instead, the neighboring H-bonded water molecules may affect it presumably through a proton relay mechanism.

2.2.5. Effect of serotonin on compound I. The reaction of low-spin heme–Aβ(WT) with H_2O_2 is carried out in the presence of a bulky substrate like serotonin and monitored by absorption spectroscopy. The absorption data reveal that in the presence of serotonin (stoichiometric amount) there is negligible formation of compound I (band at 670 nm); instead, serotonin oxidation is observed (Fig. 11). The oxidation of serotonin is characterized by the decrease of the 276 nm band characteristic of serotonin and formation of the 317 nm band characteristic of the symmetric dimer of serotonin[19,51] (Fig. 11). This indicates that in the presence of H_2O_2, compound I of low-spin heme–Aβ is the active oxidant for the oxidation of serotonin. Catalytic serotonin oxidation by low-spin heme–Aβ(WT) in the presence of H_2O_2 is also performed (Fig. S13†), and like TMB (peroxidase activity), low-spin heme–Aβ shows a significantly enhanced serotonin oxidation rate in the presence of H_2O_2 relative to control experiments, *i.e.* serotonin + H_2O_2, serotonin + H_2O_2 + heme, and serotonin + H_2O_2 + Aβ (monitored using the 317 nm band) (Fig. S13B†) that negate the association of an uncontrolled radical process caused by H_2O_2 or the involvement of adventitious metal

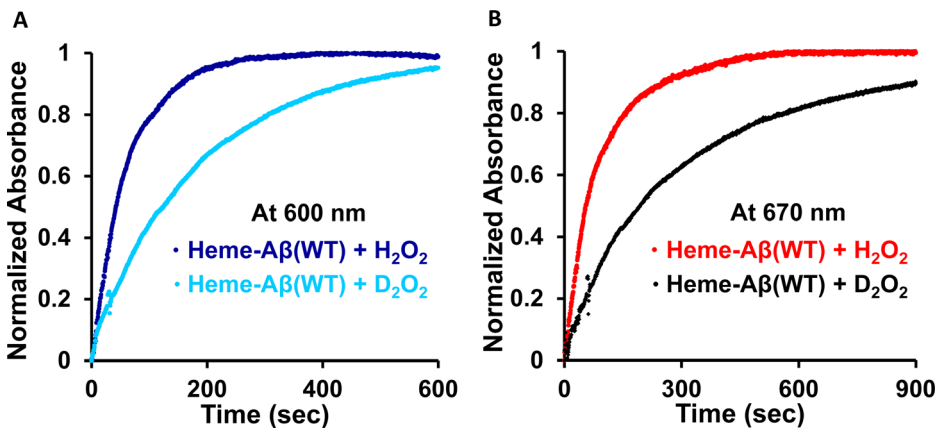

Fig. 10 (A) Overlay of the reaction kinetics for the 600 nm band formed in absorption spectroscopy in the reaction of low spin heme–Aβ(WT) with H_2O_2 (blue) and low spin heme–Aβ(WT) with D_2O_2 (cyan); (B) for the 670 nm band formed in absorption spectroscopy in the reaction of low spin heme–Aβ(WT) with H_2O_2 (red) and low spin heme–Aβ(WT) with D_2O_2 (black). The reaction is done in 100 mM phosphate buffer at pH 7.6.

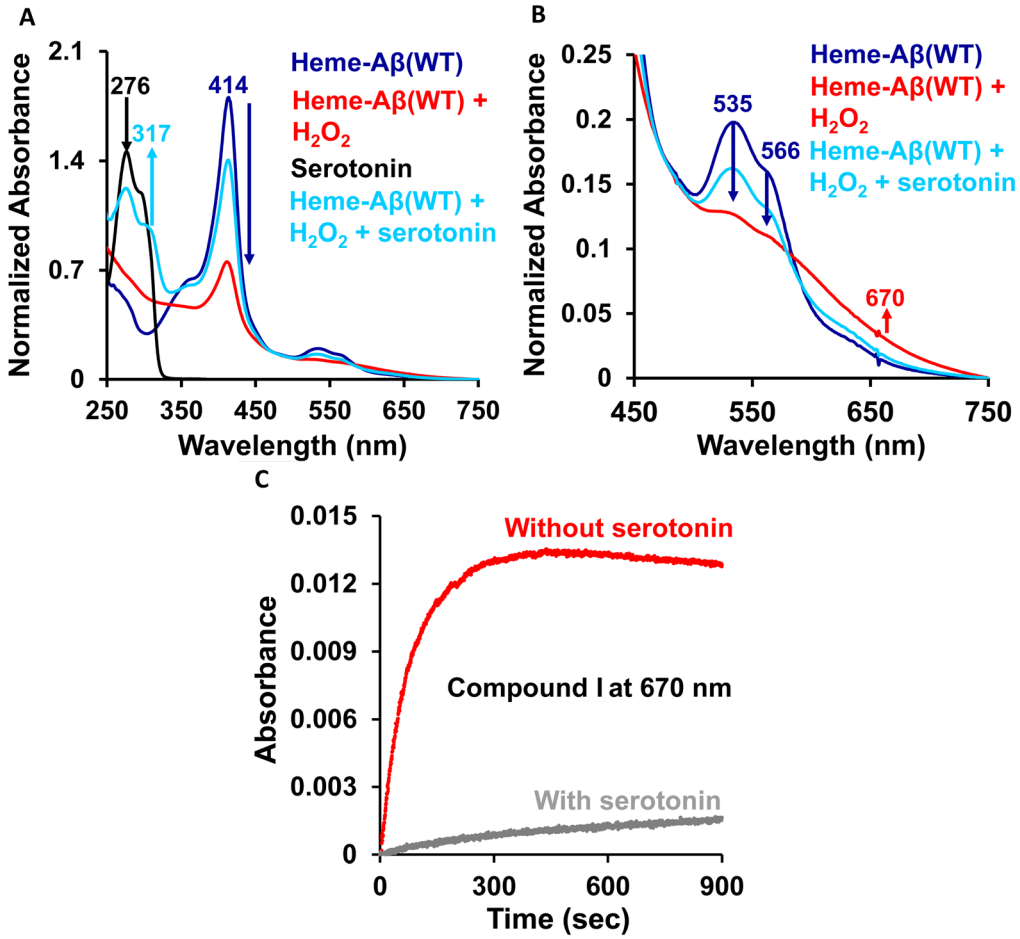

Fig. 11 (A) Absorption spectrum (full range) of low spin heme–Aβ(WT) (blue), for the reaction of low spin heme–Aβ(WT) with H_2O_2 (red), serotonin (black), low spin heme–Aβ(WT) + H_2O_2 + serotonin (cyan); (B) absorption spectrum (Q-region) of low spin heme–Aβ(WT) (blue), for the reaction of low spin heme–Aβ(WT) with H_2O_2 (red), and low spin heme–Aβ(WT) + H_2O_2 + serotonin (cyan); (C) overlay of the reaction kinetics for the 670 nm band formed in the reaction of low spin heme–Aβ(WT) with H_2O_2 in the absence of serotonin (red) and in the presence of serotonin (gray). The reaction is done in 100 mM phosphate buffer at pH 7.6.

traces in the oxidation process. This further indicates that the oxidation is caused by the compound I species generated in the reaction of low-spin heme–Aβ and H_2O_2.

3. Discussion

TMB oxidation by low-spin heme–Aβ WT and Tyr10 mutants in the presence of H_2O_2, monitored by absorption spectroscopy shows that both of these complexes carry out a two-electron oxidation of the substrate TMB to produce initially a charge–transfer complex as the one electron oxidation product followed by a diamine compound as the 2nd electron oxidation product (Fig. S2, S3 and Scheme S1†). This two-electron oxidation of the substrate TMB for low-spin heme–Aβ in the presence of H_2O_2 is typically similar to the peroxidase mechanism shown by naturally occurring peroxidases. Moreover, low-spin heme–Aβ shows significant enhancement in the rate of TMB oxidation (peroxidase activity, formation of the 652 nm band) in the presence of H_2O_2 relative to control experiments, *i.e.* TMB + H_2O_2, TMB + H_2O_2 + heme, and TMB + H_2O_2 + Aβ (Fig. S4†) that possibly exclude the association of an uncontrolled radical process generated by H_2O_2 or the involvement of adventitious metal traces in the oxidation process.

Absorption, EPR and resonance Raman spectroscopy indicate that low-spin heme–Aβ reacts with H_2O_2 to generate compound 0, which then generates compound I. Compound 0 is characterized by an absorption band at 600 nm, along with a characteristic rhombic low spin Fe^{III} EPR signal at $g_1 = 2.42$ and $g_2 = 2.06$ at 77 K (Fig. 3–5). It has characteristic ν_4 and ν_2 bands at 1375 cm^{-1} and 1591 cm^{-1}, and bands at 603 cm^{-1} and 835 cm^{-1} in the lower energy region of the resonance Raman spectrum, characterizing the Fe–O and O–O stretching, respectively (Fig. 6C, 7A, 8A and B). The bands at 603 cm^{-1} and 835 cm^{-1} undergo a large isotope shift on H/D isotope substitution indicating the involvement of protons in the formation of the Fe^{III}–OOH species *i.e.* compound 0 (Fig. 8B, S10 and S11†). The other reactive intermediate, compound I, is characterized by an absorption band at 670 nm (Fig. 3 and 4) along with resonance Raman bands, ν_4 and ν_2 at 1369 cm^{-1} and 1606 cm^{-1} respectively, in the higher energy region and 850 cm^{-1} in the lower energy region (Fig. 6, 7, 8A, C and S12A†). The 850 cm^{-1}

band shifts to 809 cm^{-1} in isotope labelled solvent (H_2O^{18}), which reaffirms the identity of compound I (Fig. 8C and S12†). This intermediate in the peroxidase catalytic cycle of low-spin heme–Aβ has been proposed to be the active oxidant responsible for its peroxidase activity (TMB oxidation), which is greater relative to the high-spin analogue. Such a difference in the peroxidase activity of high-spin and low-spin heme–Aβ can be explained by considering the stability and population of the active oxidant, compound I for the two complexes. Note that the aforementioned TMB oxidation (formation of a charge-transfer complex) can also occur due to the generation of $OH^{\bullet}$,[88–90] but for low-spin heme–Aβ, TMB oxidation is mainly attributed to the formation of compound I in the presence of H_2O_2 (peroxidase-like mechanism) as confirmed by the above spectroscopic results.

It appears that the reaction of heme–Aβ with oxidants like H_2O_2 or *m*-CPBA gets influenced by the amino acid residues present in the distal pocket of the heme center consistent with 2nd sphere effects observed in other metalloenzymes.[63–65,91] We have previously observed that the reaction of high-spin heme–Aβ with H_2O_2 or *m*-CPBA occurs too fast to accumulate any compound 0, while a relatively unstable compound I is observed.[19,22] On the other hand, the reaction of low-spin heme–Aβ and H_2O_2 is significantly slower ($\sim 10^5$ times) and the intermediates, compound 0 and compound I, are relatively stable (Fig. 3 and 4 and Table 2). The main difference between high-spin and low-spin heme–Aβ is the attachment of a distal His to the Fe^{III} center of heme in the latter case (Fig. 1), which is responsible for the slower rate of the reaction, and greater stability of the reaction intermediates. In the case of low-spin heme–Aβ, the presence of a His residue at the distal site of heme likely makes its displacement by H_2O_2 slow resulting in a slower rate of formation of compound 0.

Low-spin heme–Aβ exhibits an observed $k_H/k_D \sim 3.5$ for compound I formation. Note that the formation of compound I for high-spin heme–Aβ shows a k_H/k_D of ~2, in which case the distal arginine residue (Arg5) acts as a proton source for O–O bond heterolysis[19,22] and assists in the formation of compound I. A relatively higher KIE for the low-spin complex could likely indicate the absence of any preorganized proton transfer amino acid side chain like Arg5. This has precedence in site directed mutants of cytP450, where very high KIE is observed because of a possible water mediated proton transfer due to the lack of a preorganized proton source.[92,93]

The Tyr10 residue exhibits various redox activity in high-spin heme–Aβ complexes. It donates an electron to oxygen and is responsible for ROS generation.[6,94] Additionally, it is involved in transferring an electron to the active oxidant compound I and results in its reductive decay in high-spin heme–Aβ complexes (Scheme 1B).[19,22] However, as evident from the kinetics of WT Aβ and Tyr10Phe Aβ, it does not exhibit redox activity towards compound I in the case of low-spin heme–Aβ complexes (670 nm trace, Fig. 3D and 4D). This redox inactivity of the Tyr10 residue in low-spin heme–Aβ is also supported by our previous observations, where a 50% decrease in PROS formation was observed for low-spin heme–Aβ(WT).[42] This likely indicates that in low-spin heme–Aβ because of the coordination of a distal His to the heme–Fe center, the Tyr10 residue is no longer favorably disposed (in terms of the position and redox potential) to exhibit redox activity.

The Tyr10Phe mutant of low-spin heme–Aβ reacts with H_2O_2 resulting in the formation of compound 0 and compound I, similar to native low-spin heme–Aβ. However, the rate of formation of compound 0 corresponding to 600 nm is much faster for the Tyr10Phe mutant as compared to the native complex (Fig. S9†). Furthermore, resonance Raman data show that, although both these complexes involve the same set of intermediates *i.e.*, compound 0 and compound I, their population is higher for the low-spin heme–Aβ(Tyr10Phe) mutant as compared to the native complex (Fig. 6–8). These observations suggest that the absence of the Tyr10 residue facilitates the attack of H_2O_2 on the heme center of low-spin heme–Aβ. A higher population of the active oxidant compound I of the low-spin heme–Aβ Tyr10Phe mutant possibly accounts for its higher peroxidase activity relative to the native complex (Fig. 2B). In fact, similar observations are reported in the case of cytochrome *c*, where the stabilization of distal Fe^{III}–methionine bonding occurs through H-bonding interaction with a second sphere tyrosine residue (Tyr67).[95] It is reported that in the absence of Tyr67 in cytochrome c, the enzyme exhibits many fold increased peroxidase activity compared to native cytochrome c.[95] In the case of wild type low-spin heme–Aβ a similar scenario may be envisaged, wherein H-bonding interaction between Tyr10 and distal His (involving Tyr-O and His-N3-H) makes the Fe^{III}-His bond stronger by increasing the basicity of the histidine residue, thereby decelerating the attack by H_2O_2 (Fig. 12 and Scheme 1A). This H-bonding interaction between the phenol–O of Tyr10 and the distal N3–H of His is likely to deplete the electron density of Tyr-O, diminishing its redox activity and altering the effect of Tyr10 in low-spin heme–Aβ.

The high stability of compound I of low-spin heme–Aβ may well be attributed to the presence of water molecules in its distal pocket (Fig. 12). This prediction of the water-mediated stability of compound I of low-spin heme–Aβ is verified using a bulky

Table 2 Comparison of reaction kinetics for the intermediates formed in the reaction of heme–Aβ(1-40) (HS and LS) with peroxide

	Compound 0		Compound I	
Heme–Aβ(1-40) complexes	Formation rate (s^{-1})	Decay rate (s^{-1})	Formation rate (s^{-1})	Decay rate (s^{-1})
Heme–Aβ(WT)(HS)	Not observed	Not observed	4.70×10^{1}	24.0×10^{-1}
Heme–Aβ(Y10F)(HS)	Not observed	Not observed	5.50×10^{1}	4.00×10^{-1}
Heme–Aβ(WT)(LS)	1.60×10^{-2}	1.5×10^{-4}	8.50×10^{-3}	No decay
Heme–Aβ(Y10F)(LS)	2.35×10^{-2}	3.5×10^{-4}	10.0×10^{-3}	No decay

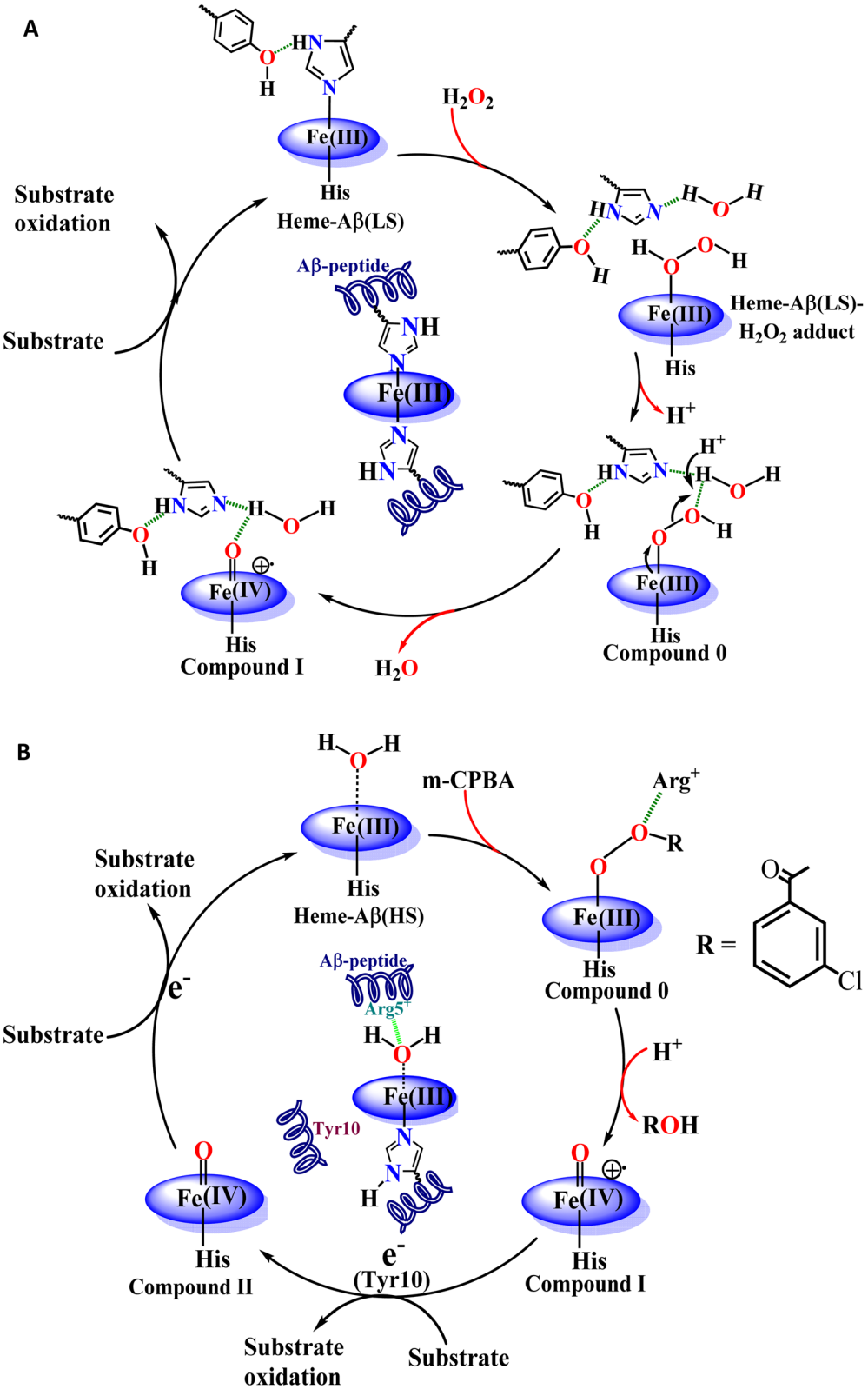

Scheme 1 Schematic representation of the catalytic cycle of the reaction of (A) low-spin heme–Aβ and H_2O_2, which undergo the formation of reactive compound 0 and compound I intermediates; (B) high-spin heme–Aβ and *m*-CPBA, which undergo the formation of reactive compound I and compound II intermediates. Compound I of both high spin and low-spin heme–Aβ is responsible for the oxidation of substrates like TMB (peroxidase activity) and neurotransmitters like serotonin.

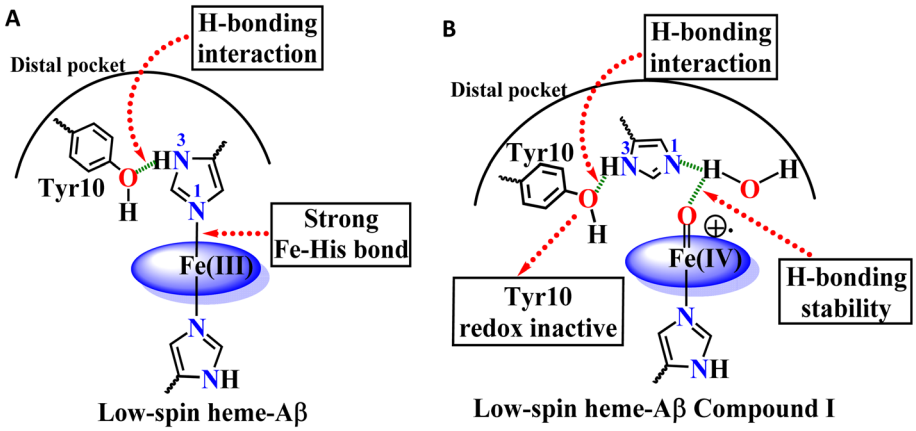

Fig. 12 (A) Demonstration of H-bonding interaction between distal His (His-N3-H) and Tyr10 in low spin heme–Aβ, which strengthens the Fe–His bond. (B) Water mediated H-bonding interaction between compound I of low spin heme–Aβ and distal His. The H-bonding interactions are demonstrated by green dashed lines.

substrate like the neurotransmitter serotonin. The results show that in the presence of serotonin, the reaction of low-spin heme–Aβ and H_2O_2 does not produce any significant amount of compound I; rather serotonin oxidation is observed (Fig. 11). Earlier theoretical studies demonstrate that similar to the low-spin heme–Aβ complex, compound I of cytP450 is found to be stable in the absence of the substrate. Such stability of compound I of cytP450 occurs due to H-bonding interaction with the neighboring water molecules. The presence of the substrate at the distal site however enhances the oxidizing capacity of compound I of cytP450 by displacing the water molecules involved in H-bonding interaction with compound I.[96] A similar H-bonding interaction from nearby water molecules, may be held by the distal His residue, is assumed for compound I of heme–Aβ low-spin (Fig. 12B and Scheme 1A), which is disrupted in the presence of the substrate, serotonin, explaining the stability of this reactive intermediate.

In contrast to the low-spin counterpart, high-spin heme–Aβ as well as its Tyr10 mutant results in a relatively unstable compound I species, which exhibits a fast decay (within a few seconds) (Table 2 and Scheme 1B).

4. Conclusion

In conclusion, low-spin bis-His heme–Aβ reacts with H_2O_2 to generate stable compound 0 and compound I as reaction intermediates. In comparison with high-spin heme–Aβ, the formation of these reactive intermediates for the low-spin complex is significantly slower and the intermediates are relatively stable. A more stable compound I of low-spin heme–Aβ therefore is mainly responsible for its enhanced peroxidase activity as compared to its high-spin analogue. Notably, the slower formation and greater stability of compound 0 and compound I for low-spin heme–Aβ are attributed to the second sphere interactions, which is different from its high-spin counterpart. Unlike high-spin heme–Aβ, the presence of distal His for the low-spin complex slows down the reaction between heme–Aβ and H_2O_2, resulting in a slower rate of formation of compound 0, whereas the absence of any preorganized proton source for low-spin heme–Aβ slows down the formation of compound I. In this case, the neighboring water molecule serves as a conduit for the necessary proton transfer (Scheme 1A). The absence of a preorganized proton source for low-spin heme–Aβ is evident from a higher KSIE value of ~3.5 for compound I formation, which is ~2 for the high-spin complex due to the presence of a preorganized Arg5 residue in the distal pocket.

The stability of compound I for low-spin heme–Aβ on the other hand depends on several factors that include the redox inactivity of the Tyr10 residue and the presence of an array of H-bonding interactions in the distal pocket (Scheme 1A). In comparison to high-spin heme–Aβ, the incapability of Tyr10 to participate in the one electron reduction of compound I for low-spin heme–Aβ can be explained by a possible H-bonding interaction of Tyr10 with distal His (Scheme 1). Such H-bonding interaction moreover strengthens the Fe–His bond, which resists the attack of H_2O_2 on the heme center (Fig. 12). Thus, in the absence of Tyr10, a greater amount of compound 0 and compound I is formed, which results in a greater peroxidase activity of the low-spin heme–Aβ Tyr10 mutant (Y10F) relative to the wild type. Another important factor for the stability of compound I is the presence of its surrounding water molecules that stabilize the intermediate through H-bonding (Fig. 12). The presence of a bulky substrate such as TMB or serotonin however diminishes this H-bonding network to make compound I reactive. This suggests that compound I of low-spin heme–Aβ can oxidize neurotransmitters like serotonin, which is important in human brain function. Importantly, among all the different forms of Aβ, the oligomers and small aggregates are found to contain significant amounts of low-spin heme–Aβ, relative to larger fibrillary aggregates. Since it is well established that the oligomeric forms of Aβ are most neurotoxic,[55–57,62,97] the presence of low spin heme–Aβ in oligomeric aggregates can be detrimental to the AD brain owing to its significantly higher peroxidase activity. This can potentially cause the oxidation of neurotransmitters, a key pathological feature of AD, making this study highly relevant to AD pathogenesis.

Author contributions

S. G. D. and A. D. supervised the project and revised the manuscript. S. G. D. and A. K. N. designed the experiments. A. K. N., M. R. and C. D. performed the experiments. All authors contributed to the data analysis and are involved in the preparation of the manuscript.

Conflicts of interest

There are no conflicts to declare.

Acknowledgements

We thank DST, SERB India, for financial support (grants EMR/2014/000392 and CRG/2020/000561). A. K. N thanks the Indian Association for the Cultivation of Science and M. R. and C. D. thank the Council of Scientific and Industrial Research for Senior Research Fellowship, respectively.

References

1 Z. Breijyeh and R. Karaman, *Molecules*, 2020, **25**, 5789.
2 H. Akiyama, S. Barger, S. Barnum, B. Bradt, J. Bauer, G. M. Cole, N. R. Cooper, P. Eikelenboom, M. Emmerling, B. L. Fiebich, C. E. Finch, S. Frautschy, W. S. Griffin, H. Hampel, M. Hull, G. Landreth, L. Lue, R. Mrak, I. R. Mackenzie, P. L. McGeer, M. K. O'Banion, J. Pachter, G. Pasinetti, C. Plata-Salaman, J. Rogers, R. Rydel, Y. Shen, W. Streit, R. Strohmeyer, I. Tooyoma, F. L. Van Muiswinkel, R. Veerhuis, D. Walker, S. Webster, B. Wegrzyniak, G. Wenk and T. Wyss-Coray, *Neurobiol. Aging*, 2000, **21**, 383–421.
3 D. J. Hayne, S. Lim and P. S. Donnelly, *Chem. Soc. Rev.*, 2014, **43**, 6701–6715.
4 M. Roy, A. K. Nath, I. Pal and S. G. Dey, *Chem. Rev.*, 2022, **122**, 12132–12206.
5 H. Jahn, *Dialogues Clin. Neurosci.*, 2013, **15**, 445–454.
6 D. Pramanik, C. Ghosh, S. Mukherjee and S. Ghosh, *Coord. Chem. Rev.*, 2013, **257**, 81–92.
7 J. Hardy and D. J. Selkoe, *Science*, 2002, **297**, 353–356.
8 F. Kametani and M. Hasegawa, *Front. Neurosci.*, 2018, **12**, 25.
9 L. M. F. Gomes, J. C. Bataglioli and T. Storr, *Coord. Chem. Rev.*, 2020, **412**, 213255.
10 K. P. Kepp, *Chem. Rev.*, 2012, **112**, 5193–5239.
11 M. A. Lovell, J. D. Robertson, W. J. Teesdale, J. L. Campbell and W. R. Markesbery, *J. Neurol. Sci.*, 1998, **158**, 47–52.
12 Z. Xiao, L. Gottschlich, R. van der Meulen, S. R. Udagedara and A. G. Wedd, *Metallomics*, 2013, **5**, 501–513.
13 A. Rauk, *Chem. Soc. Rev.*, 2009, **38**, 2698–2715.
14 A. K. Nath, A. Ghatak, A. Dey and S. G. Dey, *Chem. Sci.*, 2021, **12**, 1924–1929.
15 A. Popa-Wagner, S. Mitran, S. Sivanesan, E. Chang and A.-M. Buga, *Oxid. Med. Cell. Longevity*, 2013, **2013**, 963520.
16 C. Garza-Lombó, Y. Posadas, L. Quintanar, M. E. Gonsebatt and R. Franco, *Antioxid. Redox Signaling*, 2018, **28**, 1669–1703.
17 C. Cheignon, M. Tomas, D. Bonnefont-Rousselot, P. Faller, C. Hureau and F. Collin, *Redox Biol.*, 2018, **14**, 450–464.
18 T. Storr, *Can. J. Chem.*, 2020, **99**, 1–9.
19 I. Pal, A. K. Nath, M. Roy, M. Seal, C. Ghosh, A. Dey and S. G. Dey, *Chem. Sci.*, 2019, **10**, 8405–8410.
20 S. C. Drew, *Front. Neurosci.*, 2017, **11**, 317.
21 E. Karran, M. Mercken and B. De Strooper, *Nat. Rev. Drug Discovery*, 2011, **10**, 698–712.
22 M. Roy, I. Pal, A. K. Nath and S. G. Dey, *Chem. Commun.*, 2020, **56**, 4505–4518.
23 Y. Li, M. Nguyen, M. Baudoin, L. Vendier, Y. Liu, A. Robert and B. Meunier, *Eur. J. Inorg. Chem.*, 2019, **2019**, 4712–4718.
24 J. Zhao, Q. Shi, H. Tian, Y. Li, Y. Liu, Z. Xu, A. Robert, Q. Liu and B. Meunier, *ACS Chem. Neurosci.*, 2021, **12**, 140–149.
25 D. Chiabrando, F. Vinchi, V. Fiorito, S. Mercurio and E. Tolosano, *Front. Pharmacol.*, 2014, **5**, 61.
26 R. Gozzelino, *Curr. Alzheimer Res.*, 2016, **13**, 174–184.
27 A. K. Nath, C. Ghosh, M. Roy, M. Seal and S. Ghosh Dey, *Dalton Trans.*, 2019, **48**, 7451–7461.
28 H. Atamna and W. H. Frey, *Proc. Natl. Acad. Sci. U. S. A.*, 2004, **101**, 11153–11158.
29 H. Atamna and K. Boyle, *Proc. Natl. Acad. Sci. U. S. A.*, 2006, **103**, 3381–3386.
30 A. K. Nath and S. G. Dey, *Dalton Trans.*, 2022, **51**, 4986–4999.
31 C. Ghosh, M. Seal, S. Mukherjee and S. Ghosh Dey, *Acc. Chem. Res.*, 2015, **48**, 2556–2564.
32 F. J. Wolters, H. I. Zonneveld, S. Licher, L. G. M. Cremers, on behalf of the Heart Brain Connection Collaborative Research Group, M. K. Ikram, P. J. Koudstaal, M. W. Vernooij and M. A. Ikram, *Neurology*, 2019, **93**, e917–e926.
33 A. L. Lumsden, J. T. Rogers, S. Majd, M. Newman, G. T. Sutherland, G. Verdile and M. Lardelli, *Front. Neurosci.*, 2018, **12**, 533.
34 Y. Peng, X. Chang and M. Lang, *Int. J. Mol. Sci.*, 2021, **22**, 12442.
35 K. M. Cullen, Z. Kócsi and J. Stone, *Neurobiol. Aging*, 2006, **27**, 1786–1796.
36 P. A. Yates, R. Sirisriro, V. L. Villemagne, S. Farquharson, C. L. Masters, C. C. Rowe and For the AIBL Research Group, *Neurology*, 2011, **77**, 48–54.
37 M. Fisher, V. Vasilevko, G. F. Passos, C. Ventura, D. Quiring and D. H. Cribbs, *Stroke*, 2011, **42**, 3300–3303.
38 C.-W. Wu, P.-C. Liao, L. Yu, S.-T. Wang, S.-T. Chen, C.-M. Wu and Y.-M. Kuo, *Neurobiol. Dis.*, 2004, **17**, 367–377.
39 H. Atamna, D. W. Killilea, A. N. Killilea and B. N. Ames, *Proc. Natl. Acad. Sci. U. S. A.*, 2002, **99**, 14807–14812.
40 Y. El Khoury, A. Schirer, C. Patte-Mensah, C. Klein, L. Meyer, M. Rataj-Baniowska, S. Bernad, D. Moss, S. Lecomte, A.-G. Mensah-Nyagan and P. Hellwig, *ACS Chem. Neurosci.*, 2021, **12**, 2940–2945.
41 D. Pramanik and S. G. Dey, *J. Am. Chem. Soc.*, 2011, **133**, 81–87.
42 C. Ghosh, S. Mukherjee, M. Seal and S. G. Dey, *Inorg. Chem.*, 2016, **55**, 1748–1757.
43 L. C. Berumen, A. Rodríguez, R. Miledi and G. García-Alcocer, *Sci. World J.*, 2012, **2012**, 823493.

44 K. Sengupta, S. Chatterjee, D. Pramanik, S. G. Dey and A. Dey, *Dalton Trans.*, 2014, **43**, 13377–13383.
45 K. J. Reinikainen, H. Soininen and P. J. Riekkinen, *J. Neurosci. Res.*, 1990, **27**, 576–586.
46 L. Volicer, P. J. Langlais, W. R. Matson, K. A. Mark and P. H. Gamache, *Arch. Neurol.*, 1985, **42**, 1158–1161.
47 C. C. Meltzer, G. Smith, S. T. DeKosky, B. G. Pollock, C. A. Mathis, R. Y. Moore, D. J. Kupfer and C. F. Reynolds III, *Neuropsychopharmacology*, 1998, **18**, 407–430.
48 J. J. Rodríguez, H. N. Noristani and A. Verkhratsky, *Prog. Neurobiol.*, 2012, **99**, 15–41.
49 D. Muck-Seler, P. Presecki, N. Mimica, M. Mustapic, N. Pivac, A. Babic, G. Nedic and V. Folnegovic-Smalc, *Prog. Neuro-Psychopharmacol. Biol. Psychiatry*, 2009, **33**, 1226–1231.
50 G. M. Whitford, *Neuropsychobiology*, 1986, **15**, 133–142.
51 S. Mukherjee, M. Seal and S. G. Dey, *JBIC, J. Biol. Inorg. Chem.*, 2014, **19**, 1355–1365.
52 U. Sengupta, A. N. Nilson and R. Kayed, *EBioMedicine*, 2016, **6**, 42–49.
53 E. N. Cline, M. A. Bicca, K. L. Viola and W. L. Klein, *J. Alzheimer's Dis.*, 2018, **64**, S567–S610.
54 S. Makin, *Nature*, 2018, **559**, S4–S7.
55 A. K. Sharma, S. T. Pavlova, J. Kim, D. Finkelstein, N. J. Hawco, N. P. Rath, J. Kim and L. M. Mirica, *J. Am. Chem. Soc.*, 2012, **134**, 6625–6636.
56 Y. Huang, H.-J. Cho, N. Bandara, L. Sun, D. Tran, B. E. Rogers and L. M. Mirica, *Chem. Sci.*, 2020, **11**, 7789–7799.
57 L. Sun, H.-J. Cho, S. Sen, A. S. Arango, T. T. Huynh, Y. Huang, N. Bandara, B. E. Rogers, E. Tajkhorshid and L. M. Mirica, *J. Am. Chem. Soc.*, 2021, **143**, 10462–10476.
58 P. D. Josephy, T. Eling and R. P. Mason, *J. Biol. Chem.*, 1982, **257**, 3669–3675.
59 L. A. Marquez and H. B. Dunford, *Biochemistry*, 1997, **36**, 9349–9355.
60 C. Bacchella, J. T. Brewster, S. Bähring, S. Dell'Acqua, H. D. Root, G. D. Thiabaud, J. F. Reuther, E. Monzani, J. L. Sessler and L. Casella, *Molecules*, 2020, **25**, 5044.
61 H. Atamna, W. H. Frey II and N. Ko, *Arch. Biochem. Biophys.*, 2009, **487**, 59–65.
62 R. Khodarahmi and M. R. Ashrafi-Kooshk, *Int. J. Biol. Macromol.*, 2017, **100**, 18–36.
63 G. Smulevich, *Biochem. Soc. Trans.*, 1995, **23**, 240–244.
64 T. L. Poulos, *Chem. Rev.*, 2014, **114**, 3919–3962.
65 X. Huang and J. T. Groves, *Chem. Rev.*, 2018, **118**, 2491–2553.
66 W. D. Hewson and L. P. Hager, *J. Biol. Chem.*, 1979, **254**, 3182–3186.
67 S. Yokota and H. Fujii, *J. Am. Chem. Soc.*, 2018, **140**, 5127–5137.
68 M. Tanaka, K. Matsuura, S. Yoshioka, S. Takahashi, K. Ishimori, H. Hori and I. Morishima, *Biophys. J.*, 2003, **84**, 1998–2004.
69 I. G. Denisov, T. M. Makris and S. G. Sligar, *J. Biol. Chem.*, 2002, **277**, 42706–42710.
70 T. Kawano, S. Muto, M. Adachi, H. Hosoya and F. Lapeyrie, *Biosci., Biotechnol., Biochem.*, 2002, **66**, 646–650.
71 M. Ibrahim, I. G. Denisov, T. M. Makris, J. R. Kincaid and S. G. Sligar, *J. Am. Chem. Soc.*, 2003, **125**, 13714–13718.
72 R. Davydov, T. M. Makris, V. Kofman, D. E. Werst, S. G. Sligar and B. M. Hoffman, *J. Am. Chem. Soc.*, 2001, **123**, 1403–1415.
73 H. Kim, P. J. Rogler, S. K. Sharma, A. W. Schaefer, E. I. Solomon and K. D. Karlin, *Angew. Chem., Int. Ed.*, 2021, **60**, 5907–5912.
74 A. Singha and A. Dey, *Chem. Commun.*, 2019, **55**, 5591–5594.
75 A. Ivancich, G. Mazza and A. Desbois, *Biochemistry*, 2001, **40**, 6860–6866.
76 A. T. Smith, W. A. Doyle, P. Dorlet and A. Ivancich, *Proc. Natl. Acad. Sci. U. S. A.*, 2009, **106**, 16084–16089.
77 J. T. Colvin, R. Rutter, H. J. Stapleton and L. P. Hager, *Biophys. J.*, 1983, **41**, 105–108.
78 K. J. Paeng and J. R. Kincaid, *J. Am. Chem. Soc.*, 1988, **110**, 7913–7915.
79 V. Palaniappan and J. Terner, *J. Biol. Chem.*, 1989, **264**, 16046–16053.
80 C. M. Hosten, A. M. Sullivan, V. Palaniappan, M. M. Fitzgerald and J. Terner, *J. Biol. Chem.*, 1994, **269**, 13966–13978.
81 K. Jayaraj, A. Gold, R. N. Austin, L. M. Ball, J. Terner, D. Mandon, R. Weiss, J. Fischer, A. DeCian, E. Bill, M. Müther, V. Schünemann and A. X. Trautwein, *Inorg. Chem.*, 1997, **36**, 4555–4566.
82 K. Sengupta, S. Chatterjee and A. Dey, *ACS Catal.*, 2016, **6**, 1382–1388.
83 A. Ghatak, S. Bhunia and A. Dey, *ACS Catal.*, 2020, **10**, 13136–13148.
84 S. Kushal, C. Sudipta, S. Subhra and D. Abhishek, *Proc. Natl. Acad. Sci. U. S. A.*, 2013, **110**, 8431–8436.
85 J. R. Kincaid, A. J. Schneider and K. J. Paeng, *J. Am. Chem. Soc.*, 1989, **111**, 735–737.
86 S. Hashimoto, Y. Tatsuno and T. Kitagawa, *Proc. Natl. Acad. Sci. U. S. A.*, 1986, **83**, 2417–2421.
87 S. Bhakta, A. Nayek, B. Roy and A. Dey, *Inorg. Chem.*, 2019, **58**, 2954–2964.
88 A. Robert and B. Meunier, *ACS Nano*, 2022, **16**, 6956–6959.
89 S. Scott, H. Zhao, A. Dey and T. B. Gunnoe, *ACS Catal.*, 2020, **10**, 14315–14317.
90 B. Meunier and A. Robert, *J. Phys. Chem. C*, 2019, **123**, 28513–28514.
91 Y. Lu, S. M. Berry and T. D. Pfister, *Chem. Rev.*, 2001, **101**, 3047–3080.
92 M. Vidakovic, S. G. Sligar, H. Li and T. L. Poulos, *Biochemistry*, 1998, **37**, 9211–9219.
93 S. Chatterjee, K. Sengupta, B. Mondal, S. Dey and A. Dey, *Acc. Chem. Res.*, 2017, **50**, 1744–1753.
94 D. Pramanik, C. Ghosh and S. G. Dey, *J. Am. Chem. Soc.*, 2011, **133**, 15545–15552.
95 W. Lan, Z. Wang, Z. Yang, T. Ying, X. Zhang, X. Tan, M. Liu, C. Cao and Z.-X. Huang, *PLoS One*, 2014, **9**, e107305.
96 R. Lonsdale, J. Oláh, A. J. Mulholland and J. N. Harvey, *J. Am. Chem. Soc.*, 2011, **133**, 15464–15474.
97 A. L. Lublin and S. Gandy, *Mt. Sinai J. Med.*, 2010, **77**, 43–49.